Journal of the Korean Society for Nondestructive Testing
Vol. 25, No. 3 (2005. 6)

Ultrasonic NDE Classifications with the Gradient Descent Method and Synthetic Aperture Focusing Technique

Daewon Kim

Abstract Ultrasonic inspection methods are widely used for detecting flaws in materials. One of the more popular methods involves the extraction of an appropriate set of features followed by the use of a neural network for the classification of the signals in the feature space. This paper describes an approach which uses LMS method to determine the coordinates of the ultrasonic probe followed by the use of SAFT to estimate the location of the ultrasonic reflector. The method is employed for classifying NDE signals from the steam generator tubes in a nuclear power plant. The classification results using this scheme for the ultrasonic signals from cracks and deposits within steam generator tubes are presented.

Keywords: ultrasonic NDE, classification, least mean square, gradient descent, SAFT

I. Introduction

Ultrasonic inspections are widely used for the flaw detection of materials. The signal analysis step plays a crucial part in the data interpretation process. A number of signal processing methods have been proposed to classify ultrasonic flaw signals. The ultrasonic inspections are common tool in the nondestructive evaluation (NDE) of the steam generator tubes in nuclear power plants (Khan, 2001) which have an important role since they constitute one of the primary barriers between the radioactive and non-radioactive sides of the plant. For this reason, the integrity of the tubing is essential in minimizing the leakage of water between the two sides of the plant. In order to evaluate the structural status of a material, many researchers have proposed various kinds of methods which could classify quantitatively ultrasonic flaw signals. The classification needs an accurate and consistent determination of flawed regions and is becoming increasingly important as time goes in nuclear power plants and repair costs increase. Those methods are mainly based on the signal analysis and an automatic signal classification schemes have the potential to provide reasonable interpretation of inspection data. One of the popular approaches to perform a classification of ultrasonic signals involves the extraction of features from data followed by the use of a neural network based schemes such as a multi-layer perceptron neural network with back-propagation learning algorithm (Khan, 2001)(Polikar et al., 1998), genetic algorithm (Du-Yih, 1998). The feature extraction from an ultrasonic backscattered signal is an important part such as the computation of features that are invariant to changes in the transducer center frequency (Polikar et al., 1998), wavelet transform coefficients of ultrasound scan lines

Received : April 8, 2005. Accepted : June 9, 2005. Department of Electronics and Computer Engineering, Dankook University, San 29, Anseodong, Cheonan, Chungnam, Republic of Korea, 330-714, e-mail: drdwkim@dku.edu

(Khan, 2001; Meyer and Tuthill, 1995). The classification of ultrasonic signals also can be done alternatively by applying deconvolution approach (Demirli and saniie, 2001; Taxt, 2001). In this paper, we approached the ultrasonic signals' classification problem from a geometrical point of view and a least mean square (LMS) algorithm to estimate the parameters which are used in conjunction with synthetic aperture focusing technique (SAFT). The main objective is to develop a method for discriminating crack signals from those due to deposits. Several issues need to be studied to achieve this objective. First, investigation of the characteristics of the collected ultrasonic signals should be done. Second, a coordinate system for the probe and the tube should be developed to produce a basis for estimating the location of the probe inside the tube. Third, a technique for estimating the coordinates and its canting angle of the probe should be developed. Fourth, we need to image the geometry of the scatterers using SAFT and the technique requires reasonably accurate estimates of the location of the probe relative to the tube wall and other scatterers. Finally, the classification of the scatterer either as a crack or a deposit should be performed using its centroid. The paper is structured as follows. Section II presents a specific problem statement relating to classification of defects in steam generator tubes that are employed in nuclear power plants. Section III describes a formalism to model the probe within a tube for estimating the transducers' X,Y,Z coordinates and its canting angle. Section IV describes a mean square error (MSE) minimization procedure that employs the formalism developed in section III. The classification results of ultrasonic signals from the steam generator tubes using SAFT in conjunction with the estimates of the probe location and canting angle are then provided in section V, followed by concluding remarks in Section VI.

II. Ultrasonic Inspection of Steam Generator Tubes in Nuclear Power Plants

Steam generators are used for converting water into steam from heat produced in the reactor core in a nuclear power plant. Each steam generator contains approximately 3,000 to 16,000 tubes through which hot radioactive water flows through. Heat is conducted through the tube wall to a mixture of water and steam outside of the tube. The thermal energy transferred from the primary coolant causes the generation of steam which in turn is used for operating turbines. The harsh environmental conditions that exists within the steam generator contributes to corrosion in the tube. The tubes have to be inspected periodically to ensure that the tubes are not causing nuclear contamination of the water on the secondary side. A popular inspection technique involves the use of ultrasonic NDE methods. In inspecting the steam generator tubes, the ultrasonic transducer moves along the tube axis with water sealed between the tube wall and the transducer.

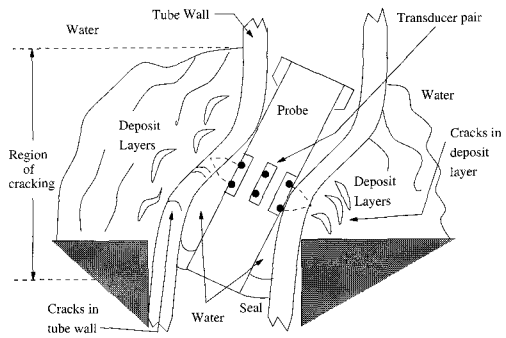

Fig. 1 Geometry of ultrasonic NDE of the steam generator tube

Figure 1 shows the ultrasonic inspection setup. This figure illustrates the tube is in the region contacting with a surrounding structure called as *tube sheet* which is the black triangle shaped geometry on both sides of the tube. There is a possibility that the tubes have cracks outside the wall in this region. Such cracks

usually extend 2 inches along the tube within and above the *tube sheet* support. Additionally, chemical precipitates and dissolved metallic compounds are deposited on the tube sheet in this region. The accumulation and expansion of the deposit material produces localized bowing of the tube immediately above the *tube sheet* (Khan, 2001). The probe has 24 pairs of transducers and each pair consists of a forward and a reverse looking element. Therefore the probe has 48 channels in total. 24 pairs of transducers collect information from the position around the tube with 15° circumferential spacing between each element pair. Each of the three sections in the probe has eight transducers for forward and reverse looking and are spaced 45° apart on the circumference. Both transducers in a pair are focused at the same spot on the outer diameter (OD) of the tube. The transducers have nominal center frequencies of 8-11 MHz (within 6dB from ~6 to ~16 MHz). The sampling frequency is 80 MHz and the thickness of the tube wall is 0.047 inches. The transducer transmits longitudinal waves with a 19.5° incidence angle. The wave travels through the water and is incident on the inner wall of the tube. When the wave arrives at the tube inner wall, mode conversion occurs and the shear wave travels into the tube wall internally at a 45° refraction angle. Signals generated by the piezoelectric elements are sampled using an 8 bit converter. The sampled and digitized signal is a 482-point signal displayed in an A-Scan format. Note that each pair of transducer is composed of two elements (forward and reverse). The signals from the two transducers are combined to form a composite A-Scan consisting of 964 sample points. The A-Scans are combined along the tube axis to obtain a 2-dimensional B-Scan image for each pair of transducers. The ultrasonic wave can be scattered by cracks present in the tube or inhomogeneities present in the chemical precipitates and dissolved metallic compounds that are deposited outside. The latter is benign and must be distinguished from cracks in the tube wall. The B-Scan image consists of signal which may represent either cracks or deposits. The signals from cracks must be discriminated from those due to deposits, since cracks in the tube wall may result in leakage of the primary coolant. The signals from deposits are benign indications and are not a source of concern. It is apparent that signals due to cracks and deposits are not significantly different. Discriminating these signals manually can be very slow and expensive. Consequently there is considerable interest in automatic methods for analyzing the data. Automated methods offer such advantages as consistency of interpretation, rapid turnaround time and lower overall costs.

III. Estimation of the Distance Between the Transducer and the Tube Wall

A method for estimating the distance between the probe and the tube wall using experimental ultrasonic data should be developed and the method involves using a geometrical model for the probe. The model allows representation of the probe coordinates and canting angle in an appropriate coordinate system and the model allows calculation of the time of flight (TOF) for reflections from the tube inner diameter (ID) for each of the eight transducers in a probe leg for a given probe location and canting angle. The probe coordinates and canting angle are estimated by minimizing the mean square error between the model TOF prediction and the observed TOFs.

A. Geometric Approach for Locating the Coordinates

The transducers are aligned circumferentially along the surface of the probe as illustrated in section II. The probe consists of three legs, each of which consists of sixteen ultrasonic transducers. The transducers are arrayed in two tiers and spaced 45° apart on the circumference. We call the eight transducers in a tier as

constituting a set. There are a total of six sets. A pair of these sets correspond to one set of forward and reverse looking elements. The probe moves forward axially along the tube axis during the inspection. Since the probe ID is less than the inner diameter of the tube the probe axis may not be aligned with the tube axis. The offset in coordinates and the canting angle with respect to the tube axis needs to be estimated. We begin by using an appropriate coordinate system.

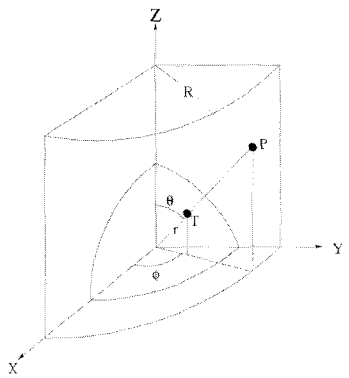

Fig. 2 Spherical and cylindrical coordinate systems for the probe and the tube

Figure 2 displays the spherical and a cylindrical coordinate system where r is a distance from the center of one set of transducers to one transducer (radius of the eight transducers' circle), R is a radius of the cylinder (tube), θ is an angle between the Z-axis and the point T, ϕ is a rotation angle of T with respect to the Z-axis, T is a location of one transducer, and P is a straight point on the cylinder from T. The Z-axis, in both cases, is aligned along the tube axis while the X-Y plane corresponds to the circumferential cross section of the tube. This figure stands for the initial setup of the probe inside the tube and the centers are matched exactly initially. We assume that one set of transducers can cant inside the cylinder with the center of the probe cross section located at (X=0, Y=0). Focusing on the spherical coordinate system, if T represents the location of one transducer in a set, the X, Y, Z coordinates are given by (Hayt, 1989),

$$X_T = r\sin\theta\cos\phi \quad (1)$$

$$Y_T = r\sin\theta\sin\phi \quad (2)$$

$$Z_T = r\cos\theta \quad (3)$$

The next step involves estimation of the coordinates of the remaining seven transducers in the set. We do so by defining the following terms in Figure 3 where $\mathbf{N}_T$ is a normal vector to the one set of transducers' circumferential cross section surface, $\mathbf{T}_i$ is a vector of i_{th} transducer, ρ_i is an angle between $\mathbf{T}_i$ and $\mathbf{T}_1$ (i=1,2,⋯..,8).

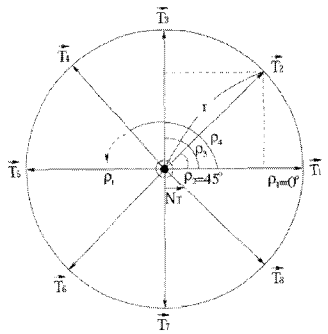

Fig. 3 Coordinates of one set of transducers

Then the normal to the surface containing the eight sensors can be determined using

$$\mathbf{N}_T = -\cos\theta\cos\phi\mathbf{a}_x - \cos\theta\sin\phi\mathbf{a}_y + \sin\theta\mathbf{a}_z \quad (4)$$

and $\mathbf{T}_1$ can be derived from equations (1),(2),(3) as

$$\mathbf{T}_1 = r\sin\theta\cos\phi\mathbf{a}_x + r\sin\theta\sin\phi\mathbf{a}_y + r\cos\theta\mathbf{a}_z \quad (5)$$

and $\mathbf{T}_2$ through $\mathbf{T}_4$ can be calculated as

$$\mathbf{T}_2 = r\left(\cos 45^\circ\sin\theta\cos\phi - \sin 45^\circ\sin\phi\right)\mathbf{a}_x + r\left(\cos 45^\circ\sin\theta\sin\phi + \sin 45^\circ\cos\phi\right)\mathbf{a}_y + r\cos 45^\circ\cos\theta\mathbf{a}_z \quad (6)$$

$$\mathbf{T}_3 = -r\sin 90^\circ\sin\phi\mathbf{a}_x + r\sin 90^\circ\cos\phi\mathbf{a}_y \quad (7)$$

$$\mathbf{T}_4 = r\left(\cos 135^\circ\sin\theta\cos\phi - \sin 135^\circ\sin\phi\right)\mathbf{a}_x + r\left(\cos 135^\circ\sin\theta\sin\phi + \sin 135^\circ\cos\phi\right)\mathbf{a}_y + r\cos 135^\circ\cos\theta\mathbf{a}_z \quad (8)$$

In order to obtain the coordinates of the remaining points which are $\mathbf{T}_5$, $\mathbf{T}_6$, $\mathbf{T}_7$ and $\mathbf{T}_8$, either $\rho_{i,(i=5,6,7,8)}$ can be replaced in equation (3) in appendix or we can multiply the X,Y and Z coordinate values of $\mathbf{T}_1$, $\mathbf{T}_2$, $\mathbf{T}_3$ and $\mathbf{T}_4$ by -1 respectively since those four vectors are symmetrical to each other through the center point, (0,0,0). However, as we mentioned at the beginning of this section, the spherical coordinates of the eight sensors can be shifted towards any direction along the X-, Y- and Z-axis. To generalize movement of the coordinates within the tube, the translation, C_x, C_y and C_z, of the X, Y and Z coordinate values should be summed with all eight vectors appropriately. The tube can be considered as a cylinder as shown in Figure 2. We assume, again, that the center is fixed at (0,0,0) for the two coordinate systems. Then, the X, Y, Z coordinates of a point P on the cylinder can be obtained as follows

$$X_P = R\cos\phi \tag{9}$$

$$Y_P = R\sin\phi \tag{10}$$

$$Z_P = R\cot\theta \tag{11}$$

The θ and ϕ in the above equations can be transformed and represented in terms of X_T, Y_T and Z_T as

$$\theta = \cos^{-1}\left[\frac{Z_T}{\sqrt{X_T^2+Y_T^2+Z_T^2}}\right] \qquad (0^\circ \le \theta \le 180^\circ) \tag{12}$$

$$\phi = \tan^{-1}\left[\frac{Y_T}{X_T}\right] \tag{13}$$

Therefore, the coordinates of P can be written in terms of the coordinates of T.

$$X_P = R\cos\left[\tan^{-1}\left(\frac{Y_T}{X_T}\right)\right] \tag{14}$$

$$Y_P = R\sin\left[\tan^{-1}\left(\frac{Y_T}{X_T}\right)\right] \tag{15}$$

$$Z_P = R\cot\left[\cos^{-1}\left(\frac{Z_T}{\sqrt{X_T^2+Y_T^2+Z_T^2}}\right)\right] \tag{16}$$

In order to obtain the coordinates for P when the center is translated, it is necessary to make use of vector algebra.

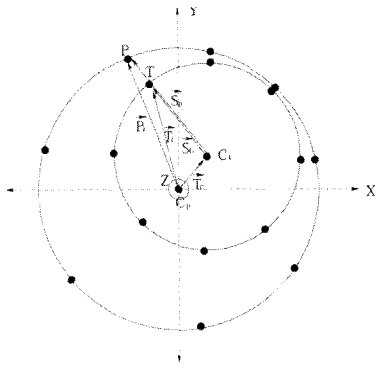

Fig. 4 Vector analysis for the coordinates of the tube

Figure 4 shows a vector analysis for the coordinates of the tube where C_P is the center of the tube, C_t is the center of eight transducers, $\mathbf{T}_i$ is a vector of i_{th} transducer (T) from the tube's center, $\mathbf{P}_i$ is a vector of the tube's ID (P) from the tube's center, $\mathbf{T}_c$ is a vector of the center for eight sensors from the center of the tube, $\mathbf{S}_{t_i}$ is a vector of i_{th} transducer (T) from the center of eight sensors, and $\mathbf{S}_{P_i}$ is a vector of the tube's ID (P) from the center of eight sensors. Figure 4 shows the circumferential cross section view of the tube with the probe inside and $\theta = 90^\circ$. The eight black small spots around the circle that are located inside, correspond to the location of each transducer (transducers are spaced 45° apart). The black spots on the outer circle represent points on the circumference of the tube. Then, $\mathbf{S}_{t_i}$ and $\mathbf{S}_{P_i}$ can be written as

$$\mathbf{T}_i - \mathbf{T}_c = \mathbf{S}_{t_i} \tag{17}$$

$$\mathbf{P}_i - \mathbf{T}_c = \mathbf{S}_{P_i} \tag{18}$$

These two vectors are related to each other via,

$$\mathbf{S}_{t_i} = \eta \mathbf{S}_{P_i} \tag{19}$$

Therefore, $\mathbf{S}_{t_i}$ and $\mathbf{S}_{P_i}$ in equation (19) can be replaced by equation (17) and (18) as

$$\mathbf{T}_i - \mathbf{T}_c = \eta(\mathbf{P}_i - \mathbf{T}_c) \tag{20}$$

From equation (20), $T_{ix}, T_{iy}, T_{iz}, T_{cx}, T_{cy}, T_{cz}$, are already known and the X, Y, Z components can be derived for each vectors so that the three equations for the four unknown parameters, $P_{ix}, P_{iy}, P_{iz}, \eta$ can be obtained.

Figure 5 shows some simulation results obtained using the model. The first column in Figure 5 shows the movement of spherical coordinates inside a cylinder obtained by changing θ, ϕ, C_x and C_y, C_z. As θ and ϕ change, the coordinates of the tube takes on an elliptical shape. The second column proves that every coordinate is on the same surface. Since all the coordinates are given, it is quite easy to calculate the distance between the two coordinate systems which is obtained as

$$D_i = \sqrt{(T_{ix} - P_{ix})^2 + (T_{iy} - P_{iy})^2 + (T_{iz} - P_{iz})^2} \tag{21}$$

where i=1,2,⋯,8. The distance D_i will be used to calculate the error with D_{m_i}, the distance estimated using TOF data calculated from the ultrasonic measurements.

B. Estimation of the Distance between the Transducers and the Inner Wall of the Tube from TOF Data

The continuous-time wavelet transform (CWT) possesses a number of properties. Some are closely related to Fourier transform properties (for example, energy conservation) while others are specific to the CWT (such as the reproducing kernel). The CWT has some localization properties, in particular, sharp time resolution and poor frequency resolution at high frequencies and good frequency resolution and poor time resolution at low frequencies. The CWT is

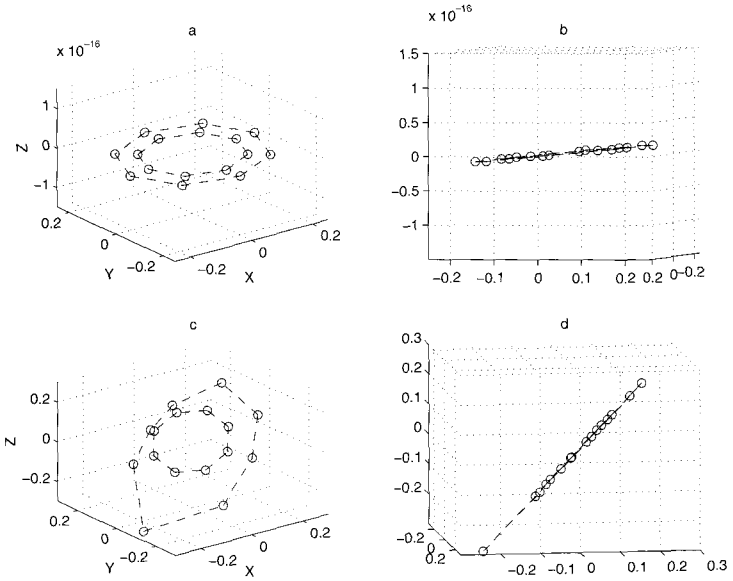

Fig. 5. Simulation of the two coordinates:
(a) $\theta = 90^\circ, \phi = 0^\circ, C_x = 0, C_y = 0, C_z = 0$ (b) Cross section view of (a) from the XZ plane,
(c) $\theta = 35^\circ, \phi = 15^\circ, C_x = 0.03, C_y = 0.05, C_z = 0$ (d) Cross section view of (c) from the XZ plane

especially valuable for analyzing signals which have high frequency components for short duration and low frequency components for extended periods (Vetterli and Kovacevic, 1995). The continuous-time wavelet transform of a signal $x(t)$ with respect to a wavelet $\psi(t)$ is defined as

$$CWT_x^{\psi}(\tau,s) = \int_{-\infty}^{\infty} x(t)\psi_{s,\tau}^{*}(t)dt \qquad (22)$$

where $\psi_{s,\tau}(t) \equiv \frac{1}{\sqrt{|s|}}\psi\left(\frac{t-\tau}{s}\right)$, s and τ are real and * denotes complex conjugation, which means that the wavelet transform is a function of two variables. The term $\frac{1}{\sqrt{|s|}}$ is used to ensure energy normalization over scales. This normalizing factor ensures that the energy stays the same for all s and τ. If the value of s is given, then the function $\psi_{s,\tau}(t)$ by the quantity τ. The time measurement with CWT has been used for nondestructive evaluation applications.

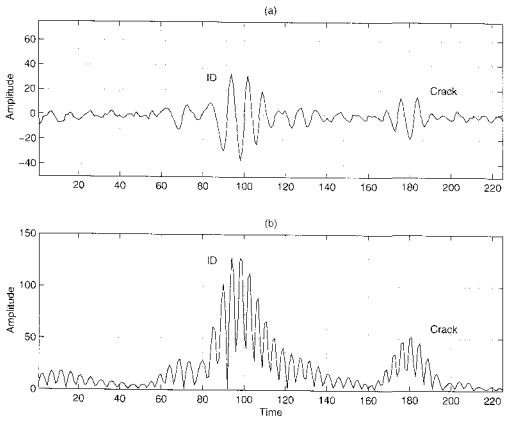

Fig. 6 A-Scan signal and its CWT (s=7)

Figure 6 shows an A-Scan of the real data and the result at which it has the maximum amplitude as obtained from the CWT of the signal using the Morlet wavelet as the mother wavelet. The signal is windowed to capture reflections from the crack and deposit regions. The time position where it has maximum amplitude is used for estimation of the location of the ID of the tube. In order to calculate the distance between the transducer and ID of the tube, the velocity of the ultrasonic wave needs to be considered. As explained in section II, the ultrasonic wave travels through water and the metal tube. The signal velocities in low alloy steel (tube) and water are 3150 m/s and 1480 m/s respectively which means the speed of ultrasound in tube is higher than in water. It is known apriori that 0.047 inches corresponds to 63 pixels in the B-Scan. This corresponds to the thickness of the tube wall. The time required for the wave to traverse 0.047 inches in water can be obtained using Snell's law (Schmerr, 1998),

$$\frac{T_M}{T_W} = \frac{V_W}{V_M} = \frac{1}{\varepsilon} = \frac{\sin 19.5^{\circ}}{\sin 45^{\circ}} = 0.4721 \qquad (23)$$

where T_M, T_W is the time in metal and water and V_M, V_W is the velocity in metal and water respectively. From the Snell's law in (23), $T_W = T_M \times \varepsilon$, therefore, the distance corresponding to 63 time pixels in metal, which is known to correspond to the thickness of the tube (0.047 inches), is the same as 63ε time pixels in water from the B-Scan image where $\varepsilon = 2.1183$.

Table I Distance for one pixel in metal and water

	In Metal	In Water
0.047 inch	63 pixels (known)	63ε pixels
One pixel	0.000746 inch	0.000352192 inch

Table I shows the distances in water and metal for one pixel. It can be noticed that the signal's travel velocity in metal is approximately twice faster than that in water. Therefore, 0.000352192 is multiplied with the measured TOF to obtain the distance in inches. The angle of incidence should also be considered to calculate the shortest distance from the transducer to the ID. The incident angle is 19.5°

consequently we need to multiply $\cos 19.5^{\circ}$ with the measured distance to compute a shortest distance.

IV. Mean Square Error Minimization using the Least Mean Square Algorithm

We use the least mean square (LMS) method to arrive at the estimates of the probe coordinates and canting angle. The LMS algorithm is widely used in a number of applications due to its computational simplicity.

A. MSE Minimization using the Steepest Descent Method

The gradient of mean square error (MSE) is employed to estimate the canting angle as well as C_x and C_y. The angle ϕ cannot be estimated from the data due to rotational symmetry. The sum of all the distances between the probe and the tube wall can be estimated from the B-Scan image. However the data does not contain any information to estimate ϕ. Although the direction of Z-axis can be fixed, the X, Y axis cannot be fixed to allow estimation of ϕ. In addition, C_z does not need to be estimated since we are not interested in estimating the axial position of the probe. We are therefore interested in computing the gradient with respect to θ, C_x and C_y only. The steepest descent algorithm can be considered as an efficient gradient type method because it works with the true gradient vector, and not with an estimate. Therefore the performance of other gradient type algorithms can at most be close to the performance of the steepest descent method (Solo and Kong, 1995). Using this iterative minimization procedure, the optimum value for θ, C_x and C_y which give the minimum error can be achieved by orienting the search in a direction that is opposite to that of the gradient of E (which defines the direction of maximum increase). The steepest descent algorithm updates the coefficients using

$$\delta_{i+1} = \delta_i - \mu \left. \frac{\partial V(\delta)}{\partial \delta} \right|_{\delta=\delta_i} \tag{24}$$

Since $\nabla_{\delta} V$ defines the direction of maximum increase in the function, the function $V(\delta)$ can be minimized by recursively calculating $\nabla_{\delta} V$ and adjusting δ until it reaches a minimum. μ is called the convergence factor since the choice affects the convergence behavior.

B. Results of Optimization

Estimates of C_x, C_y and θ were obtained using the procedure outlined in preceding section using data obtained by Knolls Atomic Power Laboratory (KAPL). Typical B-Scan image is shown in Figure 7 which represents data obtained during the inspection of a straight length of tube.

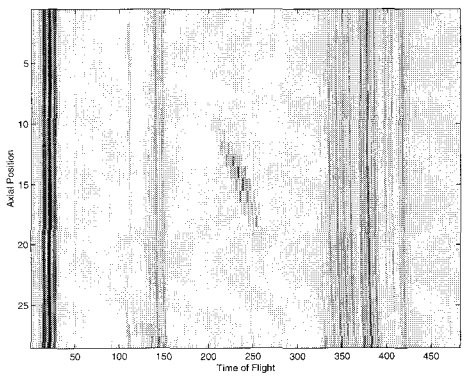

Fig. 7 B-Scan image of the data collected from a straight section

Table II shows estimates of θ, C_x, C_y and the minimum MSE for the data shown in Figure 7. The table shows estimates from the ten different axial positions for a tier of the probe each containing forward and reverse looking transducers. Table II shows that the probe canting angle, θ, as well as C_x and C_y have not changed appreciably in a straight length of

tube as the probe moves along the tube axis since θ is close to 90°.

F1 through F6 and R1 through R6 mean the forward and reverse looking sensors at the axial position 1 through 6 respectively. This is consistent with the physical geometry of the problem where the tube ID is 0.406 inches and the diameter of the probe is 0.325 inches. There is consequently very little room for the probe to tilt/cant within the tube in a straight section. Those three values, θ, C_x, and C_y can be verified if they are reasonable or not by comparing the calculated and measured distances between the tube inner wall and the eight transducers at a certain axial position.

The distances are displayed in Figures 8 where 8(a), 8(b) show the distances for the forward and reverse looking elements respectively. The calculated distances are also plotted in the figures and those are reasonably consistent with the measured distance.

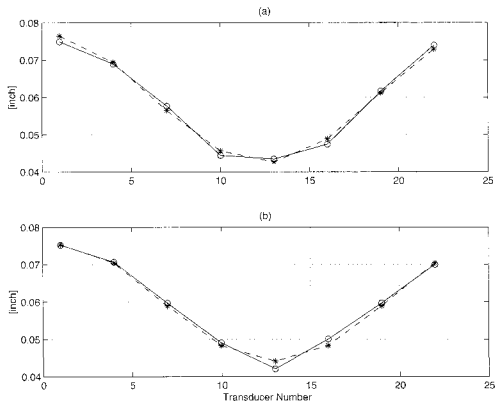

Fig. 8 Comparison of the calculated(∗) and measured(∘) distances for data displayed in Fig. 7: (a)Forward transducer for Fig. 7, (b)Reverse transducer for Fig. 7

Table II Optimum values of θ, C_x, C_y estimated using the steepest descent method for data displayed in Fig. 7

	θ	C_x	C_y	MSE
F1	88.54°	-0.0167	0.0028	1.1431×10^{-6}
R1	88.54°	-0.0157	1.6817×10^{-3}	1.2015×10^{-6}
F2	88.57°	-0.0169	0.0029	1.2247×10^{-6}
R2	88.53°	-0.0157	1.9923×10^{-3}	1.1908×10^{-6}
F3	88.57°	-0.0169	0.0029	1.2243×10^{-6}
R3	88.54°	-0.0153	1.3534×10^{-3}	1.1138×10^{-6}
F4	88.61°	-0.0171	0.0023	1.1884×10^{-6}
R4	88.54°	-0.0155	1.3827×10^{-3}	1.1445×10^{-6}
F5	88.54°	-0.0166	0.0024	1.2988×10^{-6}
R5	88.54°	-0.0160	1.3288×10^{-3}	1.0138×10^{-6}
F6	88.57°	-0.0169	0.0029	1.2247×10^{-6}
R6	88.54°	-0.0159	1.2119×10^{-3}	1.2703×10^{-6}
F7	88.57°	-0.0169	0.0037	1.3013×10^{-6}
R7	88.71°	-0.0162	1.5248×10^{-3}	1.1138×10^{-6}
F8	88.60°	-0.0169	0.0025	1.4511×10^{-6}
R8	88.73°	-0.0160	1.7568×10^{-3}	1.5143×10^{-6}
F9	88.57°	-0.0169	0.0029	1.2247×10^{-6}
R9	88.73°	-0.0162	1.8636×10^{-3}	1.4779×10^{-6}
F10	88.16°	-0.0166	0.0033	1.3404×10^{-6}
R10	88.45°	-0.0162	1.7434×10^{-3}	1.7274×10^{-6}

V. Results of Classification using SAFT

Synthetic aperture focusing techniques (SAFT) process data so as to simulate a larger transducer to obtain better resolution and signal to noise ratio (SNR) (Masri et al., 1994). A-Scan signals are first time-shifted in order to align the reflections from scatterers. The time-shifted signals are then added up coherently so that the point of focus coincides resulting in the reconstruction of an image with improved SNR. The estimated values of C_x, C_y and θ are used in SAFT. The value of θ allows computation of the true angle of incidence from the transducer and the beam spread angle at the tube wall at each axial position inside the tube.

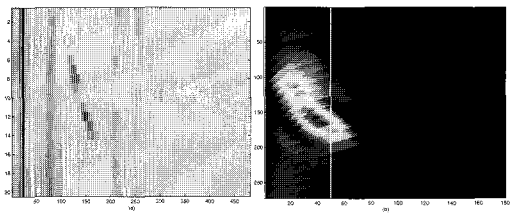

Fig. 9 (a)68% crack, (b)SAFT result for (a) in a straight section

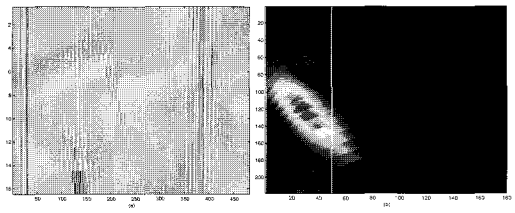

Fig. 10 (a)47% crack, (b)SAFT result for (a) in a straight section

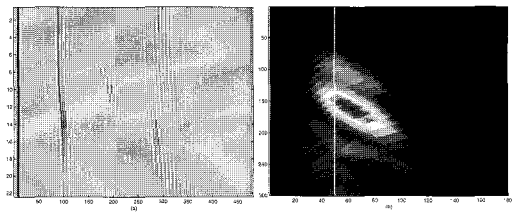

Fig. 11 (a)45% deposit, (b)SAFT result for (a) in a straight section

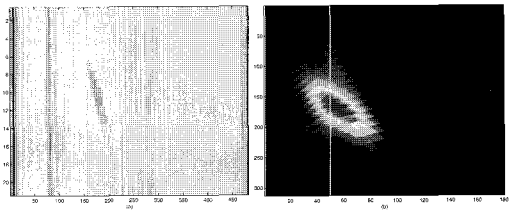

Fig. 12 (a)18% deposit, (b)SAFT result for (a) in a straight section

Figures 9 through 12 show the images obtained, after processing for cracks and deposits. In all these figures, (a) represents the input B-Scan image while (b) represents the reconstructed image obtained using SAFT. In each of the figures 9(b)-12(b), the reconstructed image is displayed such that the ID of the tube is the left edge of the image. This allows a closer look of the flaw. The white vertical lines located at 1 and 50 on the X-axis indicate the positions of ID and OD of the tube respectively. The elliptical-shaped spots in Figures 9(b)-12(b) indicate the locations of flaws of interest. Figures 9 and 12 show results obtained from a straight section of the tube. For Figures 9(b), 10(b), the flaw part is located mainly inside the OD. Consequently those are classified as cracks in the tube. We can recognize two cracks in the tube in Figure 9.
In Figures 11(b), 12(b), the flaw is located generally outside the OD and consequently those are classified as deposits. These SAFT results show similar classification performance compared to the results obtained without the estimate of the beam spread angle since the probe is located in a straight section of the tube.

VI. Conclusion

In this paper, we developed a method for discriminating crack signals from those due to deposits for ultrasonic NDE of steam generator tubes in nuclear power plants. The characteristics of the ultrasonic signals collected from cracks and deposits are studied and a

coordinate system for the probe and the tube has been developed to produce a basis for estimating the location of the probe inside the tube and the distance between them has been calculated. The distance between the transducer and the tube wall from the collected data has been measured using continuous-time wavelet transform and consideration of the velocity effects. Expressions for gradient of the MSE with respect to the probe coordinates and canting angle have been derived and the gradient is incorporated in LMS algorithm to obtain the optimum values of probe coordinates and canting angle. The classification results show how estimates of the parameters can be used in conjunction with the SAFT to improve the SNR of the image. Future work can be focused on finding a method for estimating the centroid of the scatterer with respect to the tube wall so that it is used as a basis for determining more accurately if the scatterer is a crack located within the tube wall or is due to inhomogeneity in the deposit.

Acknowledgements

The author would like to thank Dr. Satish Udpa and Dr. Lalita Udpa at Michigan State University for his and her help. This work was supported in part by the Knolls Atomic Power Laboratory (KAPL) in USA.

References

Demirli R., Saniie J. (2001) Model-based estimation of ultrasonic echoes part II: nondestructive evaluation applications, *IEEE Transactions on Ultrasonics, Ferroelectrics, and Frequency Control*, Vol. 48. No. 3, pp. 803-811

Du-Yih T. (1998) Classification of heart diseases in ultrasonic images using neural networks trained by genetic algorithms, *Proceedings of the Fourth International Conference on Signal Processing*, Vol. 2, pp. 1213-1216

Hayt W. H. (1989) *Engineering Electromagnetics,* McGraw-Hill Book Company, New York, USA, pp. 125-128

Khan A. (2001) *Defect Classification for Steam Generator Tubes of a Nuclear Power Plant using Ultrasonic Nondestructive Techniques,* M. S. Thesis, Iowa State University, Ames, IA, USA, pp. 23-26

Masri W., Mina M., Udpa S. S., Udpa L., Lord W. (1994) Synthetic Aperture Focusing Technique Using the Envelope Function for Ultrasonic Imaging, *Review of Progress in Quantitative NDE*, Vol. 14A, pp. 909-914

Meyer E., Tuthill T. (1995) Bayesian classification of ultrasound signals using wavelet coefficients, *Proceedings of the IEEE 1995 National Aerospace and Electronics Conference*, Vol. 1, pp. 240-243

Polikar R., Udpa L., Udpa S. S., Taylor T. (1998) Frequency invariant classification of ultrasonic weld inspection Signals, *IEEE Transactions on Ultrasonics, Ferroelectrics and Frequency Control*, Vol. 45, No. 3, pp. 614-625

Schmerr L. W. Jr. (1998) *Fundamentals of Ultrasonic Nondestructive Evaluation,* Plenum Publishing Corporation, New York, USA, pp. 167-169

Solo V., Kong X. (1995) A*daptive Signal Processing Algorithms*, Prentice Hall, New York, USA, pp. 56-58

Taxt T. (2001) Three-dimensional blind deconvolution of ultrasound images, *IEEE Transactions on Ultrasonics, Ferroelectrics, and Frequency Control*, Vol. 48, No. 4, pp. 867-871

Vetterli M., Kovacevic J. (1995) *Wavelets and Subband Coding*, Prentice Hall PTR, New York, USA, pp. 78-79

Appendix

The vectors $\mathbf{T}_1$ *through* $\mathbf{T}_8$

In order to verify if $\mathbf{N}_T$ is truly normal to the surface, we can check that $\mathbf{N}_T \cdot \mathbf{T}_1 = \mathbf{0}$. Next, $\mathbf{T}_2$ can be represented in terms of $\mathbf{T}_1$ and $\mathbf{T}_3$ as

$$\mathbf{T}_2 = \alpha \mathbf{T}_1 + \beta \mathbf{T}_3 \tag{1}$$

where the α and β are some constants which can be represented by r, ρ_2 and the magnitudes of $\mathbf{T}_1$ and $\mathbf{T}_3$. At this point, $\mathbf{T}_3$ can be written in terms of $\mathbf{N}_T$ and $\mathbf{T}_1$ as

$$\mathbf{T}_3 = \mathbf{N}_T \times \mathbf{T}_1 \tag{2}$$

Then $\mathbf{T}_3$ in equation (1) can be replaced by equation (2) as

$$\begin{aligned} \mathbf{T}_2 &= \alpha \mathbf{T}_1 + \beta (\mathbf{N}_T \times \mathbf{T}_1) \\ &= r \cdot \frac{\mathbf{T}_1}{|\mathbf{T}_1|} \cdot \cos\rho_2 + r \cdot \frac{\mathbf{N}_T \times \mathbf{T}_1}{|\mathbf{N}_T \times \mathbf{T}_1|} \cdot \sin\rho_2 \\ &= \mathbf{T}_1 \cdot \cos\rho_2 + (\mathbf{N}_T \times \mathbf{T}_1) \cdot \sin\rho_2 \end{aligned} \tag{3}$$

In the case of $\mathbf{T}_2$, ρ_2 is 45°. Likewise, for $\mathbf{T}_3$ and , ρ_3 and ρ_4 can be replaced by 90° and 135° respectively.